CORA Cork Open Research Archive
Cartlann Taighde Oscailte Chorcaí

Title	Multi-stimuli selectivity CuO/V2O5 memristive devices for broadband sensing applications
Authors	Sharmila, Balachandar;Dwivedi, Priyanka
Publication date	2026-08-28
Original Citation	Balachandar, S. and Dwivedi, P. (2026) 'Multi-stimuli selectivity CuO/V2O5 memristive devices for broadband sensing applications', IEEE Sensors Journal. https://doi.org/10.1109/JSEN.2026.3725743
Type of publication	Article (peer-reviewed)
Link to publisher's version	10.1109/jsen.2026.3725743
Rights	© 2026, IEEE. Personal use of this material is permitted. Permission from IEEE must be obtained for all other uses, in any current or future media, including reprinting/republishing this material for advertising or promotional purposes, creating new collective works, for resale or redistribution to servers or lists, or reuse of any copyrighted component of this work in other works.
Download date	2026-11-04 12:27:49
Item downloaded from	https://hdl.handle.net/10468/19317



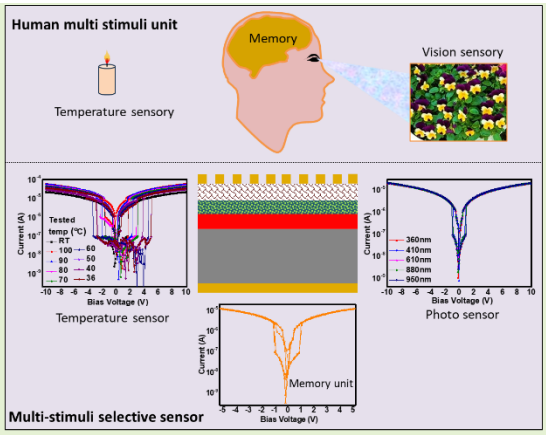
UCC
University College Cork, Ireland
Coláiste na hOllscoile Corcaigh

This article has been accepted for publication in IEEE Sensors Journal. This is the author's version which has not been fully edited and content may change prior to final publication. Citation information: DOI 10.1109/JSEN.2026.3725743

Multi-Stimuli Selectivity CuO/V_2O_5 Memristive Devices for Broadband Sensing Applications

Sharmila B[1,2], Graduate student *Member, IEEE*, and Priyanka Dwivedi[1*], Senior, *Member, IEEE*

***Abstract*—This paper presents a wafer scalable synthesis process for the efficient CuO/V_2O_5 based memristive devices for broadband sensing applications. The memristive devices are tested using three different sensing stimuli to analyze the trigger selectivity and widen the real time sensing applications. The electrical, broadband optical, and thermal stimuli are used to stimulate the CuO/V_2O_5 heterostructure based memristive devices. The tested devices have demonstrated the bipolar resistive sweep with enhancement in the performance metrics like current switching ratio, resistance switching ratio and set/reset time for the thermal stimuli as compared to the other tested stimuli. The demonstrated memristor has shown the current switching ratio of ~0.8×10^3 for the thermal stimuli (90°C optimum temperature) which is ~ 38 and 28 times higher than the electrical and optical stimulation respectively. The testing results highlight the potential of the proposed devices for scalable batch processing for mass production of multifunctional broadband sensing devices.**



***Index Terms*— Microfabrication, Broadband Sensing, Memristive devices, Fast switching speed, Heterostructure, Thermal stimuli**

I. Introduction

THE traditional complementary metal oxide semiconductor (CMOS) devices have complex circuitry with more capacitors to mimic the bioinspired synaptic operations. These traditional technologies used the von Neumann architecture, which has a distinct unit for memory and processing. Due to these distinct units, traditional architectures are lagging in terms of more transmission delay, space and area related constraints [1, 2]. Therefore, it is important to develop a device which has capability to perform parallel operations like sensing, processing and storage just like biological neural systems. The biological neural networks have the capability to perform parallel operations such as sense, process and store simultaneously [3]. In recent years, researchers have devoted their efforts to mimic the biological synaptic behavior using volatile memristor, nonvolatile memristor and different synaptic transistor structures. The devices are inspired by the biological sensory neural system that can sense, interpret and store the processed information in a parallel manner. Similarly, memristive devices have the potential to replicate the synaptic behavior of the human brain functionality. Memristive devices are considered as suitable replacement for the traditional silicon based neuromorphic computing systems [4]. The storage and erasing of the memristor depends on the formation and rupture of the conductive filament. This formation and rupture depend on the applied polarity of the bias voltage (positive or negative). This process depends on the material thickness, oxygen vacancies, direction of the bias, device operating temperature, etc. There are few researchers who have investigated the impact of the bias voltage using various aspects. X. Ding et al. reported the impact of film thickness on resistive switching behavior of the TiO_x/HfO_2 based resistive random-access memory (RRAM). The 10 nm and 30 nm TiO_x film thickness-based RRAM devices were fabricated using radio frequency (RF) sputtering process. It was concluded from the experiment that the 30 nm TiO_x film based RRAM device has improved performance than the 10 nm TiO_x film [5]. T. H. Park et al. fabricated Ta_2O_5 film with various thickness. The Ta_2O_5 film having a 0.5 nm has shown the gradual change in the resistance switching behavior and high repetition rate. However, the film having a thickness of 1–2 nm showed an abruptness, less reliability and degradation in the resistance rate [6]. K. Rudrapal et al. reported the impact of the oxygen vacancy using the WO_{3-x} memristors on resistive switching properties. The tested device exhibited the non-formable characteristics depending on the stoichiometric form [7]. G. Tarsoly et al.

This work was supported by the Design Innovation Centre (Grant No. 001/MHRD/0215). The authors would like to thank the Indian Institute of Technology (IIT) Kanpur for providing characterization facilities.

Sharmila B is with the [1]Indian Institute of Information Technology (IIIT) Sri City, Chittoor – 517646, India and [2]Tyndall National Institute, Ireland. Priyanka Dwivedi is with the Indian Institute of Information Technology (IIIT) Sri City, Chittoor – 517646, India (*E-mail: priyanka.dwivedi@iiits.in).

XXXX-XXXX © XXXX IEEE. Personal use is permitted, but republication/redistribution requires IEEE permission.
See http://www.ieee.org/publications_standards/publications/rights/index.html for more information.
Authorized licensed use limited to: UNIVERSITY COLLEGE CORK. Downloaded on September 23,2026 at 13:01:04 UTC from IEEE Xplore. Restrictions apply.
© 2026 IEEE. All rights reserved, including rights for text and data mining and training of artificial intelligence and similar technologies. Personal use is permitted, but republication/redistribution requires IEEE permission. See https://www.ieee.org/publications/rights/index.html for more information.

This article has been accepted for publication in IEEE Sensors Journal. This is the author's version which has not been fully edited and content may change prior to final publication. Citation information: DOI 10.1109/JSEN.2026.3725743

demonstrated TiO_2/a-IGZO bilayers memory devices. The stoichiometry and performance of the device was controlled by annealing temperature. The 350°C annealed device has shown the widest memory window than other tested devices [8]. In addition, there are few reports that describe the impact of the device operating temperature on the resistive switching. C. Yu Han et al. reported that the Pt/VO_2/Pt memristor structure was fabricated on a flexible kapton polyimide substrate. The demonstrated device has shown the high endurance, low operating current and good bending stability of $>10^4$ cycles, <130 µA and $>10^3$ respectively. The tested device was stimulated using 20 to 40 °C. The results concluded that the tested devices have resemblance of biological warm receptor characteristics during the elevated temperature [9]. Q. Duan et al. reported the fusion of the haptic VO_2 volatile memristor having serial connection with piezoresistive sensor to mimic the biospired haptic-temperature fusion [10]. There are various types of metal oxides and their heterostructure were reported for the memristor device fabrication. In the family of metal oxides, CuO and V_2O_5 are well known for fabricating memristor based applications due to their advanced electrical and optical properties. CuO is p-type metal oxide which has an advantage of low fabrication cost, ease of synthesis, band gap tunability, high chemical/mechanical stability, etc. [11]. Similarly, V_2O_5 is another important n-type metal oxide material that has high optical/chemical stability, multiple oxidation states, etc. [12]. There are different research works that have been done using CuO, V_2O_5 and their heterojunction for memristor applications. The V_2O_5/CuO heterojunction based memristor includes benefits of both V_2O_5 and CuO for various fields. There were several research articles stating that the heterostructure based memristive architectures yield better performance than the single materials. However, CuO/V_2O_5 heterostructure for memristive device fabrication and testing the trigger selectivity for the memristive application is not explored in detail. Therefore, this paper demonstrates the CuO/V_2O_5 heterostructure based memristive devices tested under the various stimulation conditions such as electrical, broadband optical stimulation and thermal stimulation for broadband sensing applications. In addition, in this paper we have explored the impact of multiple stimuli which is one of the gray domains yet to be explored.

This paper analyzes the impact of multi stimuli selectivity resistive switching behavior of the CuO/V_2O_5 based memristive devices during electrical, optical and thermal stimulation. The CuO/V_2O_5 devices were fabricated and characterized using the standard microfabrication process and microstructural/morphological analysis respectively. The tested device has shown bipolar resistive switching for applied stimulation. The tested device has offered the current switching ratio of 0.21×10^2, 0.28×10^2 and 0.8×10^3 for the electrical, optical and thermal stimulation respectively. The device has shown to be more responsive towards the thermal stimuli as compared to the other tested stimuli (electrical and optical). In addition, the tested device shows the ultrafast set/reset time of 40.4/40.3 µs for thermal stimulation.

II. Experimental Section

A. Device Fabrication

This section presents the steps involved during the CuO/V_2O_5 device fabrication and material synthesis optimization (Fig. 1). In order to fabricate the devices, p-type single side polished (SSP) <100> silicon wafers were used for process. The wafers were cleaned using standard Radio Corporation of America (RCA) cleaning techniques. As the multiple devices are fabricated on the same substrate, the isolation of individual devices has been considered as the primary step. In this regard, the thermal oxidation layer was grown using the standard dry wet dry thermal oxidation technique at 1050 °C. Further, the thin layer of vanadium (V) with the purity of 99.9% was deposited using the DC magnetron sputtering followed by annealing at 550°C in air at 90 mins. This process yields the formation of V_2O_5 on SiO_2/Si substrate. In the next step copper (Cu-99.9% purity) was deposited on the V_2O_5/SiO_2/Si substrate through a sputtering process. In the next step Cu thin film was oxidized at 550°C for 90 mins. The final step of device fabrication was related to the metal electrode formation. The Au/Cr metal electrodes were fabricated using lift-off process on top of the CuO/V_2O_5 sensing layer.

B. Material Characterization and Multi-Stimuli Selectivity Measurements

The surface morphology and CuO/V_2O_5 nanostructure formation details were obtained from the CARL Zeiss EVO 50's scanning electron microscope (SEM). The Raman spectrum was extracted using the LabRAM HR Evolution RAMAN spectrometer (Horiba). The Raman spectrum was performed by illuminating the CuO/V_2O_5 sample using 514 nm argon-ion laser with the grating of 1800 l/mm. Further, the Phillips X'Pert, PRO-PW 3040 diffractometer was used to analyze the crystalline structure of the fabricated sample. Further, the trigger selectivity test was performed using the source measurement unit (2614 B) associated with the probe station and heater. Thorlabs light source (SLS 201) was used as an optical stimulation which has variation in the wavelength ranges such as 360 nm, 410 nm, 610 nm, 880 nm and 950 nm.

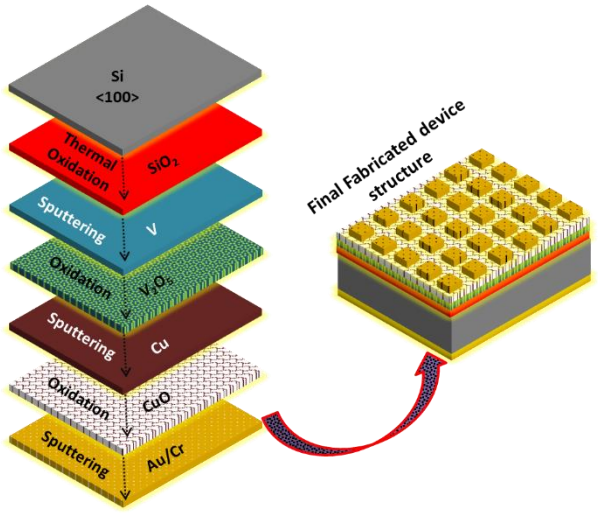


Fig. 1: Device fabrication flow of the CuO/V_2O_5 device

Authorized licensed use limited to: UNIVERSITY COLLEGE CORK. Downloaded on September 23,2026 at 13:01:04 UTC from IEEE Xplore. Restrictions apply.
© 2026 IEEE. All rights reserved, including rights for text and data mining and training of artificial intelligence and similar technologies. Personal use is permitted, but republication/redistribution requires IEEE permission. See https://www.ieee.org/publications/rights/index.html for more information.

This article has been accepted for publication in IEEE Sensors Journal. This is the author's version which has not been fully edited and content may change prior to final publication. Citation information: DOI 10.1109/JSEN.2026.3725743

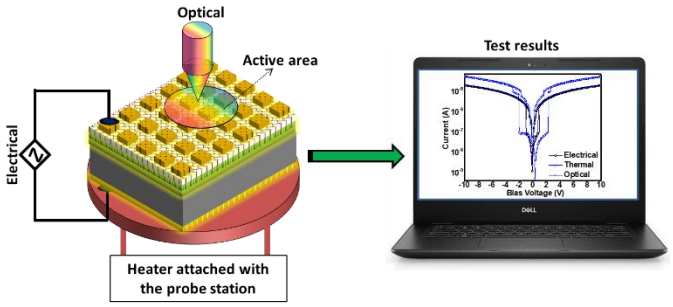


Fig. 2. Demonstration of the applied stimulation (not to scale)

The wide spectrum was chosen to demonstrate broadband sensing applications. Fig. 2 depicts the sensing test steps in the presence of various stimulation.

III. Results and Discussion

This section presents the morphological and microstructural analysis of the sample CuO/V_2O_5 sample. In addition, this section presents the results of the CuO/V_2O_5 based memristor structure under the various stimuli.

A. Morphological and Microstructural analysis

Fig. 3(a-b) demonstrates the SEM micrograph of the fabricated CuO/V_2O_5 sample. It was observed that the CuO/V_2O_5 has uniform formation over the substrate. Further the sample was analyzed using SEM micrographs that demonstrate CuO/V_2O_5 in nanostructured form. From these micrographs we can conclude that the nanostructures are formed uniformly across the sample. Fig. 3(c) and Fig. 3(d) shows the Raman spectrum and X-ray diffraction (XRD) pattern of the fabricated sample at room temperature. The tested sample has shown the Raman peaks at 79 cm^{-1}, 102.8 cm^{-1}, 388 cm^{-1}, 520 cm^{-1}, 856 cm^{-1} and 914 cm^{-1}. The peak at 102 cm^{-1} occurs due to the A_g external bending vibration of V_2O_5 [13, 14]. The B_{2g} LM(a) (Vb) mode was observed at 388 cm^{-1} [15]. Along with all peaks due the Si substrate the peak was observed at 520 cm^{-1}. The crystallography details of the fabricated sample were analyzed using XRD spectrum ranging from 10° to 80°.

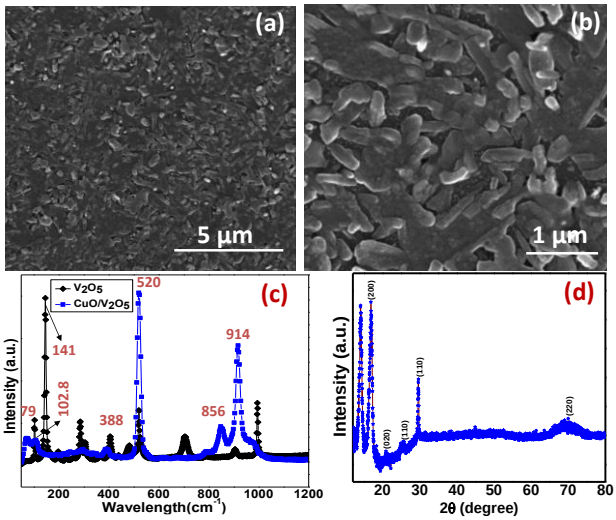


Fig. 3. Morphological view of the sample (a) 5 µm (b) 1 µm (c) Raman Spectroscopy (d) XRD

The XRD pattern was recorded at the glazing angle of 0.5. The XRD peak occurred at 14°, 15.9°, 18.3°, 26°, 29.6° and 68.8° at room temperature. The peak at 26° is related to the (110) crystal plane of V_2O_5 [16]. The peak at 29.6° corresponds to the (110) lattice plane of the copper oxide [17]. The peak at 15.9° occurred due to the (200) plane of the V_2O_5 [18]. Other peaks at 18.3° and 68.8° represent the (020) and (220) plans of the CuO respectively [19] [20]. Further, using the Debye–Scherrer equation, the average crystallite size of the synthesized CuO/V_2O_5 sample was calculated to be ~ 26 nm.

B. Multi-Stimuli Selectivity Test for Broadband Sensing

This section presents the impact of the various stimulation like electrical, optical and thermal stimulation on memristive behavior. Initially, DC electrical stimuli with voltage sweep of -10 V to 10 V was used to stimulate the devices (Fig. 4(a)). The voltage 0 V to 10 V has been applied to the device at ~1.8 V, the device has switched from high resistance state (HRS) to low resistance state (LRS). It was understood from Fig. 4(a) that the current was low at HRS and high at LRS state. Further, negative voltage stimuli were applied to the device. When the reset voltage is less than the applied voltage. Then the device will switch back to its original state. Similarly, the device was stimulated using the optical stimuli which had various wavelengths such as 360 nm, 410 nm, 610 nm, 880 nm and 950 nm. It was observed that the device has shown the minimum variation for optical stimuli (Fig. 4(b)). The switching ratio of the device was improved as compared to the electrical stimulation. The performance metrics like responsivity and detectivity are calculated using broadband spectrum. The responsivity is the ability of the device to produce photocurrent for the applied optical stimulation. Detectivity is the lowest detection limit of the device. The tested device has shown the highest sensitivity towards the 950 nm as compared to the other tested wavelengths, with responsivity and detectivity of 232 mA/W and 3.27×10^{10} Jones respectively. Further, the device was stimulated using thermal stimulation. In this regard, the operating temperature of the device was increased from room temperature. At each 10°C rise in temperature, the device has shown enhancement in current order as well as the switching ratio.

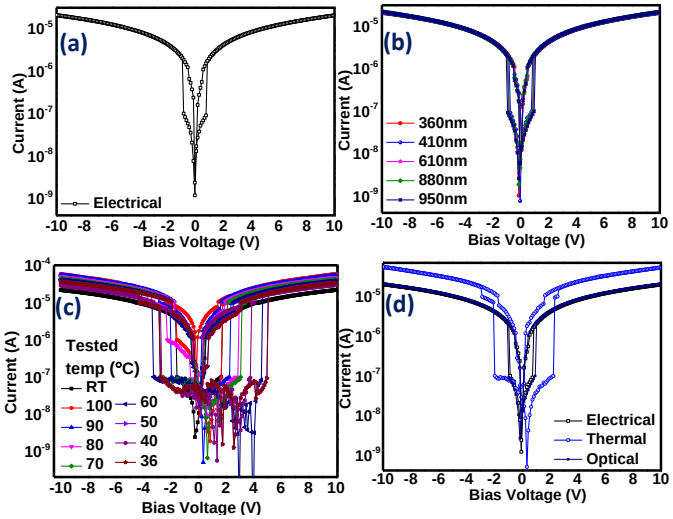


Fig. 4. Resistive switching of the fabricated devices (a) Electrical stimuli (b) Optical stimuli (c) Thermal stimuli (d) Comparative plot

Authorized licensed use limited to: UNIVERSITY COLLEGE CORK. Downloaded on September 23,2026 at 13:01:04 UTC from IEEE Xplore. Restrictions apply.
© 2026 IEEE. All rights reserved, including rights for text and data mining and training of artificial intelligence and similar technologies. Personal use is permitted, but republication/redistribution requires IEEE permission. See https://www.ieee.org/publications/rights/index.html for more information.

This article has been accepted for publication in IEEE Sensors Journal. This is the author's version which has not been fully edited and content may change prior to final publication. Citation information: DOI 10.1109/JSEN.2026.3725743

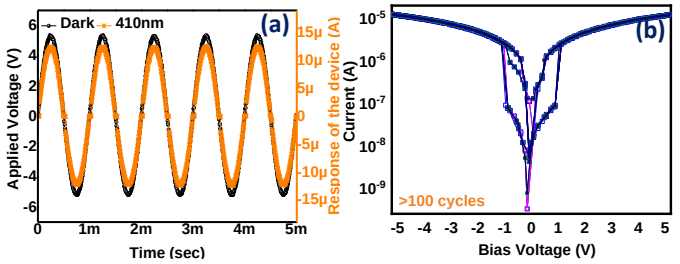


Fig. 5. (a) Resistive switching properties of the fabricated device under sine wave (b) Response of the device and repeatability test for >100 cycles

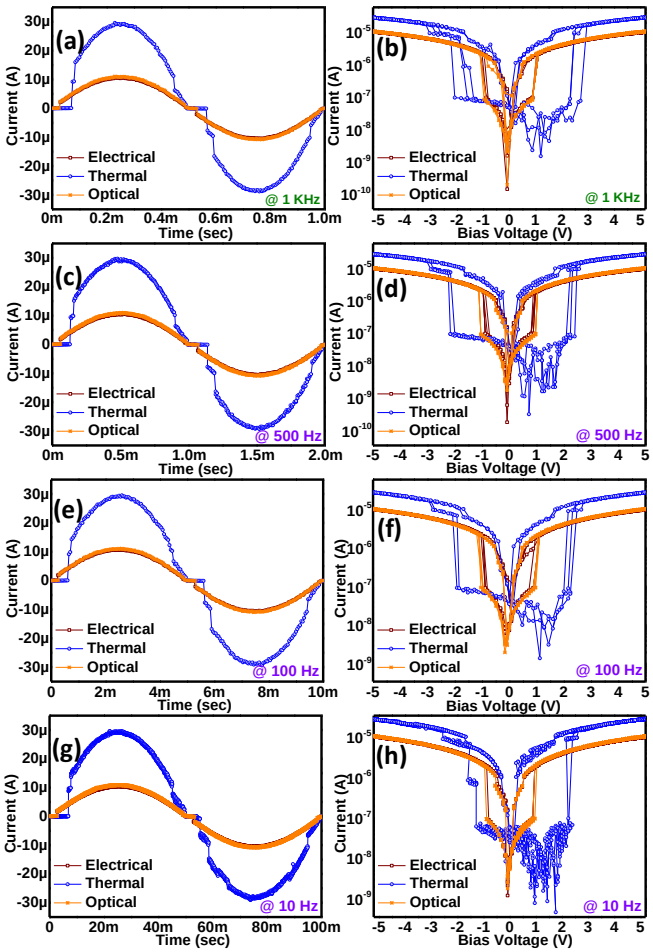


Fig. 6. Resistive switching during the modulated frequency (a-b) 1 kHz (c-d) 500 Hz (e-f) 100 Hz (g-h) 10 Hz

It was observed that the device performance was degraded at 100°C. Therefore, it has been concluded that 90°C is optimum temperature for the device performance (Fig. 4(c)). Fig. 4(d) depicts the comparative plot of the resistive switching characteristics under the various stimulation. In addition, the device was stimulated using AC sweep under the various stimulation. In this experiment sine wave was used with peak-to-peak voltage of ±5 V. Fig. 5(a) and Fig. 5(b) depicts the applied sine wave and the corresponding response of the device. The stability and endurance of the fabricated devices. To confirm the reproducibility, the device was tested for more than 100 cycles.

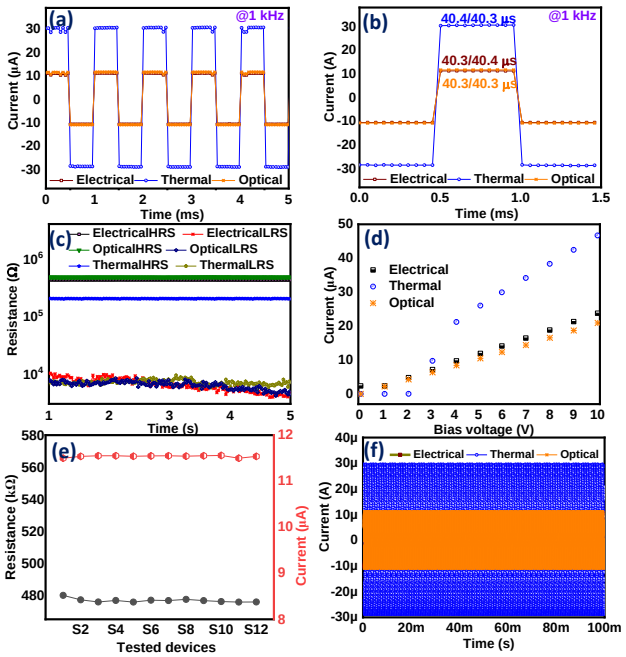


Fig. 7. Impact of the various sensing stimuli on the device performance parameters (a) Set and reset process (b) Response speed calculation (c) HRS and LRS (d) Current with respect to the bias voltage (e)D2D variability test (f) C2C variability test

TABLE I

COMPARATIVE STUDY OF THE PROPOSED DEVICE SENSING WITH STATE OF ART WORK

Material	Stimuli/Sensing	On/Off ratio	Repeatability Cycles	Ref.
V_2O_5/NiMnIn	Thermal			[21]
CuO/ZnO	Electrical	10^3	100 cycles	[22]
CuO NW	Electrical	-	1	[23]
CuO nanowire	Electrical	10^3	30 cycles	[24]
Si/CuO	Electrical Optical	-	-	[25]
CuO	Electrical	-		[26]
CuO/(AgO)	Electrical	10	40 cycles	[27]
CuO/V_2O_5	Electrical	0.21×10^2	>100 cycles	[This work]
	Optical	0.28×10^2	>100 cycles	
	Thermal	0.8×10^3	>100 cycles	

The test results confirm that the device is highly repeatable for all the tested cycles. Fig. 6(a-h) depicts the sinusoidal wave

Authorized licensed use limited to: UNIVERSITY COLLEGE CORK. Downloaded on September 23,2026 at 13:01:04 UTC from IEEE Xplore. Restrictions apply.
© 2026 IEEE. All rights reserved, including rights for text and data mining and training of artificial intelligence and similar technologies. Personal use is permitted, but republication/redistribution requires IEEE permission. See https://www.ieee.org/publications/rights/index.html for more information.

This article has been accepted for publication in IEEE Sensors Journal. This is the author's version which has not been fully edited and content may change prior to final publication. Citation information: DOI 10.1109/JSEN.2026.3725743

under the various stimulation conditions like electrical, optical and thermal with modulated frequency. It was observed that the device has shown variation in terms of current switching ratio, set/reset voltage, etc. The device has shown the current switching ratio of 0.21×10^2, 0.28×10^2 and 0.8×10^3 for the electrical, optical and thermal stimulation respectively. The device has shown the symmetrical and asymmetrical resistive characteristics during the electrical/optical and thermal stimulation respectively. It was observed that the device offered a set/reset voltage of 2.7/2 V (thermal stimuli) and 0.8/0.8 V (electrical and optical). Further, the device was stimulated using the ±5 V to store and erase the data from the CuO/V_2O_5 memristive devices (Fig. 7(a)). Further, the data was stored using + 5 V followed by the data erase using -5 V. The set and reset time were calculated under the various stimulation. The device has shown the set/reset time of 40.4/40.3 µs, 40.3/40.4 µs and 40.3/40.3 µs for the thermal, electrical and optical stimulation respectively (Fig. 7(b)). Fig. 7(c) shows the impact of the resistance states: HRS/LRS during electrical, optical and thermal stimuli. This HRS and LRS experiment was performed for the presynaptic voltage stimuli of 10 V and 0 V respectively. It was observed that the device has shown high resistance to optical stimuli as compared to the other tested stimuli. The device offered the HRS/LRS ratio of 0.68×10^2 (optical), 0.44×10^2 (electrical) and 0.27×10^2 (thermal). Fig. 7(d) represents the current with respect to the bias voltage under the various stimulation conditions. The tested device has shown the enhanced current corresponding to the increase in the bias voltage. Table I represents the comparison of the proposed device to the existing state of art works. In addition, we have tested the device to device (D2D) variation to confirm the wafer scalability of the fabricated devices. In this regard, twelve devices were taken from each side of the fabricated 2" silicon wafer. The devices were tested for the current and resistance at room temperature. The tested devices have shown similar results which further confirms the scalability of the developed process (Fig. 7(e)). Therefore, the device fabrication process is wafer scalable. Furthermore, the cycle to cycle (C2C) variation was tested for 100 cycles under various stimulation. The device shows stable output for tested 100 cycles (Fig. 7(f)).

C. Memristive Device Mechanism

The mechanism of the fabricated devices depended on the photosensing and memristive behavior under electrical, optical and thermal stimuli. First the device was stimulated by electrical stimulation. At the ambient atmosphere, the device observes the atmospheric oxygen; this oxygen reacts with the free electrons of the sensing layer. This process results in the generation of negatively charged oxygen molecules which leads to the generation of low conductive depletion regions (Equ.(1)). Due to this limited charge carrier generated under applied electric stimuli. This current is called the dark current of the device under test. Further, optical illumination was applied on the device, which results in the generation of electron and hole pairs (Equ. (2)). These holes reacted with the negatively charged oxygen molecules. During this process, there is excess generation of free electrons (Equ. (3)). These free electrons move toward the electrode which results in the enhancement of photocurrent. As the fabricated device has a heterostructure, therefore recombination of holes and electrons

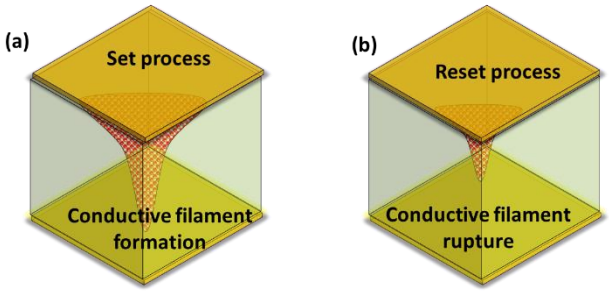


Fig. 8. Mechanism of the fabricated device (a) set process (b) reset process

is not possible at the interface [28]. On the other hand, the memristive behavior formation and rupture will happen due to the oxygen vacancies. The mechanism of the memristor was divided into three types based on the applied stimuli such as electrical, optical and thermal. During the electrical stimulation, there will be movement of the charge carriers from the top electrode to bottom electrode. During that time there will be the formation of conductive filament between the electrodes (Fig. 8(a)). This is known as the set process. In the case of optical and thermal stimuli the set process may occur due to the photogenerated carriers and thermally generated charge carriers respectively. Further, the negative electrical stimulation was used to remove the data present in the memristor. It is known as the reset process of the memristor (Fig. 8(b)) [29,30]. During the electrical stimulation, the field could not sufficiently drive the ions/defects from the top to bottom electrode. Whereas thermal stimulation helps to modify the crystalline nature of the material. The heating of the device enhances oxygen-vacancy motion from the top to bottom electrode. Which results in formation of the filament between the top and bottom electrodes [31,32]. This way the fabricated device's performance was tested for the different stimuli.

$$O_2(g) + e^- = O_2^-(adsorped) \quad \ldots\ldots(1)$$
$$h\nu = h^+ + e^- \quad \ldots\ldots(2)$$
$$h^+ + O_2^-(adsorped) = O_2(g) + e^- \quad \ldots\ldots(3)$$

IV. Conclusion

This paper presented the successful demonstration of CuO/V_2O_5 based efficient memristive devices for broadband sensing. Trigger selectivity of the device was tested using electrical, optical and thermal stimulation. The tested devices have shown enhanced performance for the thermal stimulation as compared to the other tested stimuli. The demonstrated memristor has shown the current switching ratio of 0.21×10^2 (electrical), 0.28×10^2 (optical) and 0.8×10^3 (thermal). The device offered low set/reset voltage 0.8/0.8 V during electrical/optical stimulation as compared to the thermal stimulation (2.7/2 V). The developed process can be used for a wide range of sensing applications like photo sensing, memristive and temperature sensor related field applications.

Acknowledgment

The authors acknowledge the Indian Institute of Technology Kanpur for providing characterization facilities. The authors also thank the Design Innovation Centre (Grant No. 001/MHRD/0215) for financial support.

Authorized licensed use limited to: UNIVERSITY COLLEGE CORK. Downloaded on September 23,2026 at 13:01:04 UTC from IEEE Xplore. Restrictions apply.
© 2026 IEEE. All rights reserved, including rights for text and data mining and training of artificial intelligence and similar technologies. Personal use is permitted, but republication/redistribution requires IEEE permission. See https://www.ieee.org/publications/rights/index.html for more information.

This article has been accepted for publication in IEEE Sensors Journal. This is the author's version which has not been fully edited and content may change prior to final publication. Citation information: DOI 10.1109/JSEN.2026.3725743

REFERENCES

[1] J. Y. Kwon, J. E. Kim, J. S. Kim, S. Y. Chun, K. Soh, and J. H. Yoon, "Artificial sensory system based on memristive devices," *Exploration*, vol. 4, no. 1, Nov. 2023, doi: 10.1002/exp.20220162.

[2] Q. Duan *et al.*, "Artificial Multisensory Neurons with Fused Haptic and Temperature Perception for Multimodal In-Sensor Computing," *Advanced Intelligent Systems*, vol. 4, no. 8, Mar. 2022, doi: 10.1002/aisy.202200039.

[3] O. A. M. López, A. M. López, and J. Crossa, "Fundamentals of artificial neural networks and deep learning," in *Springer eBooks*, 2022, pp. 379–425. doi: 10.1007/978-3-030-89010-0_10.

[4] V. K. Sangwan *et al.*, "Visualizing thermally activated memristive switching in percolating networks of Solution-Processed 2D semiconductors," *Advanced Functional Materials*, vol. 31, no. 52, Sep. 2021, doi: 10.1002/adfm.202107385.

[5] X. Ding, L. Liu, Y. Feng, and P. Huang, Effect of TiO_x Film Thickness on Resistive Switching Behavior of $TiN/TiO_x/HfO_2/Pt$ RRAM Device. 2019, pp. 1–2. doi: 10.23919/snw.2019.8782976.

[6] T. H. Park *et al.*, "Thickness effect of ultra-thin Ta_2O_5 resistance switching layer in 28 nm-diameter memory cell," *Scientific Reports*, vol. 5, no. 1, Nov. 2015, doi: 10.1038/srep15965.

[7] K. Rudrapal, M. Biswas, B. Jana, V. Adyam, and A. R. Chaudhuri, "Tuning resistive switching properties of WO_{3-x}-memristors by oxygen vacancy engineering for neuromorphic and memory storage applications," *Journal of Physics D Applied Physics*, vol. 56, no. 20, p. 205302, Mar. 2023, doi: 10.1088/1361-6463/acc258.

[8] G. Tarsoly, J.-Y. Lee, F. Shan, and S.-J. Kim, "Switching facilitated by the simultaneous formation of oxygen vacancies and conductive filaments in resistive memory devices based on thermally annealed TiO_2/a-IGZO bilayers," *Applied Surface Science*, vol. 601, p. 154281, Jul. 2022, doi: 10.1016/j.apsusc.2022.154281.

[9] C. Y. Han *et al.*, "Characterization and modelling of flexible VO_2 MOTt Memristor for the artificial spiking warm receptor," *Advanced Materials Interfaces*, vol. 9, no. 19, Jun. 2022, doi: 10.1002/admi.202200394.

[10] Q. Duan *et al.*, "Artificial Multisensory Neurons with Fused Haptic and Temperature Perception for Multimodal In-Sensor Computing," *Advanced Intelligent Systems*, vol. 4, no. 8, Mar. 2022, doi: 10.1002/aisy.202200039.

[11] S. B, A. Kr. Sarkar, and P. Dwivedi, "Self-Powered, Ultra-Fast CuO nanocubes surface for broadband photosensing applications," *IEEE Sensors Journal*, vol. 24, no. 16, pp. 25558–25564, Aug. 2024, doi: 10.1109/jsen.2024.3416214.

[12] S. B, A. K. Dikshit, and P. Dwivedi, "Device reliability and effect of temperature on memristors: nanostructured V_2O_5," *IEEE Transactions on Device and Materials Reliability*, vol. 24, no. 2, pp. 329–334, Apr. 2024, doi: 10.1109/tdmr.2024.3392634.

[13] M. Picuntureo, J. A. García-Merino, R. Villarroel, and S. A. Hevia, "The synthesis of sponge-like V_2O_5/CNT hybrid nanostructures using vertically aligned CNTs as templates," *Nanomaterials*, vol. 14, no. 2, p. 211, Jan. 2024, doi: 10.3390/nano14020211.

[14] R. Basu and S. Dhara, "Spectroscopic study of native defects in the semiconductor to metal phase transition in V_2O_5 nanostructure," *Journal of Applied Physics*, vol. 123, no. 16, Dec. 2017, doi: 10.1063/1.5011112.

[15] R. Baddour-Hadjean, M. B. Smirnov, V. Y. Kazimirov, K. S. Smirnov, and J.-P. Pereira-Ramos, "The Raman spectrum of the γ′-V_2O_5 polymorph: a combined experimental and DFT study," *Journal of Raman Spectroscopy*, vol. 46, no. 4, pp. 406–412, Feb. 2015, doi: 10.1002/jrs.4660.

[16] C.-C. Wang, C.-L. Lu, F.-S. Shieu, and H. C. Shih, "Structure and photoluminescence properties of thermally synthesized V_2O_5 and Al-Doped V_2O_5 nanostructures," *Materials*, vol. 14, no. 2, p. 359, Jan. 2021, doi: 10.3390/ma14020359.

[17] G. Shi, J. Liu, B. Chen, Y. Bao, and J. Xu, "Phase-controlled growth of cubic phase CuO nanoparticles by chemical vapor deposition," *Physica Status Solidi (A)*, vol. 214, no. 10, Jun. 2017, doi: 10.1002/pssa.201700041.

[18] Y. Xiao, M. Pan, J. Zou, R. Guo, X. Zeng, and W. Ding, "Surfactant induced formation of flower-like V_2O_5 microspheres as cathode materials for rechargeable magnesium batteries," *Ionics*, vol. 25, no. 12, pp. 5889–5897, Jul. 2019, doi: 10.1007/s11581-019-03139-6.

[19] C. Tamuly, I. Saikia, M. Hazarika, and M. R. Das, "Reduction of aromatic nitro compounds catalyzed by biogenic CuO nanoparticles," *RSC Advances*, vol. 4, no. 95, pp. 53229–53236, Oct. 2014, doi: 10.1039/c4ra10397a.

[20] D. Zhu, L. Wang, W. Yu, and H. Xie, "Intriguingly high thermal conductivity increment for CuO nanowires contained nanofluids with low viscosity," *Scientific Reports*, vol. 8, no. 1, Mar. 2018, doi: 10.1038/s41598-018-23174-z.

[21] K. Kaushlendra and D. Kaur, "Enhanced Synaptic Characteristics under Applied Magnetic Field in V_2O_5/NiMnIn-Based Switching Device for Neuromorphic Computing," *ACS Applied Electronic Materials*, vol. 5, no. 6, pp. 3362–3372, Jun. 2023, doi: 10.1021/acsaelm.3c00387.

[22] Y. Huang *et al.*, "CuO/ZnO memristors via oxygen or metal migration controlled by electrodes," *AIP Advances*, vol. 6, no. 2, Feb. 2016, doi: 10.1063/1.4942477.

[23] N. Z. Fan, N. X. Fan, A. Li, and N. L. Dong, *Resistive switching in copper oxide nanowire-based memristor*. 2012. doi: 10.1109/nano.2012.6322196.

[24] K.-D. Liang *et al.*, "Single CuO_X Nanowire Memristor: Forming-Free Resistive Switching Behavior," *ACS Applied Materials & Interfaces*, vol. 6, no. 19, pp. 16537–16544, Aug. 2014, doi: 10.1021/am502741m.

[25] K. Leng, Y. Wan, Y. Fu, L. Wang, and Q. Wang, "SI/CuO Heterojunction-Based Photomemristor for reconfigurable, Non-Volatile, and Self-Powered In-Sensor computing," *Small*, vol. 20, no. 28, Feb. 2024, doi: 10.1002/smll.202309945.

[26] M. J. Therese, V. Mishra, M. S. R. Rao, and T. Dixit, "First-Principles calculations to establish the functionality of Self-Connected Point-Defect migrations in N-ZNO- and P-CuO-Based memristive devices," *IEEE Transactions on Electron Devices*, vol. 70, no. 11, pp. 6026–6033, Sep. 2023, doi: 10.1109/ted.2023.3317000.

[27] S. Zou, P. Xu, and M. C. Hamilton, "Resistive switching characteristics in printed Cu/CuO/(AgO)/Ag memristors," *Electronics Letters*, vol. 49, no. 13, pp. 829–830, Jun. 2013, doi: 10.1049/el.2013.1302.

[28] Hanggara Sudrajat, Maya Nobatova; "Heterojunction photocatalysts: where are they headed?," *RSC Appl. Interfaces,* Vol. 2, pp. 599–619, 2025, doi: 10.1039/d5lf00037h.

[29] K. Ranganathan, M. Fiegenbaum-Raz, and A. Ismach, "Large-Scale and robust multifunctional vertically aligned MOS_2 Photo-Memristors," *Advanced Functional Materials*, vol. 30, no. 51, Sep. 2020, doi: 10.1002/adfm.202005718.

[30] S. Pravinraj, M.-L. Chen, S. Adat, and Y.-W. Wang, "Optoelectronic Stimuli-Driven Switchable Memristor with Multilevel Resistance States for Neuromorphic Vision Sensors," *Journal of Materials Chemistry C*, Jan. 2024, doi: 10.1039/d4tc01796j.

[31] L.-C. Shih, Z.-S. Liao, G. Cherkashinin, E. Piros, L. Alff, and J.-S. Chen, "Thermally Activated Negative Differential Resistance VO x Memristor with Switchable Rate and Leaky Integrate-and-Fire Spiking Dynamics," *ACS Nano*, vol. 19, no. 42, pp. 37165–37174, Oct. 2025, doi: 10.1021/acsnano.5c11481.

[32] A. Gooran-Shoorakchaly, S. S. Sharif, and Y. M. Banad, "Investigating the effect of electrical and thermal transport properties on oxide-based memristors performance and reliability," *Scientific Reports*, vol. 15, no. 1, p. 18646, May 2025, doi: 10.1038/s41598-025-02909-9.

Authorized licensed use limited to: UNIVERSITY COLLEGE CORK. Downloaded on September 23,2026 at 13:01:04 UTC from IEEE Xplore. Restrictions apply.
© 2026 IEEE. All rights reserved, including rights for text and data mining and training of artificial intelligence and similar technologies. Personal use is permitted, but republication/redistribution requires IEEE permission. See https://www.ieee.org/publications/rights/index.html for more information.